Journal of Organometallic Chemistry 975 (2022) 122422

Contents lists available at ScienceDirect

Journal of Organometallic Chemistry

journal homepage: www.elsevier.com/locate/jorganchem

Novel photothermal therapy using multi-walled carbon nanotubes and platinum nanocomposite for human prostate cancer PC3 cell line

Mohammed Faiad Naief[a], Yousif H. Khalaf[b], Ahmed Mishaal Mohammed[c,*]

[a] Basic Science Section, College of Agricultural Engineering Science, University of Baghdad, Baghdad, Iraq
[b] Department of Clinical Lab. Sciences, College of Pharmacy, University Of Anbar, Ramadi, Iraq
[c] Department of Chemistry, College of Science, University Of Anbar, Ramadi, Iraq

ARTICLE INFO

Article history:
Received 19 March 2022
Revised 27 May 2022
Accepted 6 June 2022
Available online 7 June 2022

Keywords:
MWCNTs
Pt-NPs
Photothermal therapy
Prostate cancer treatment
Plasmon resonance

ABSTRACT

Multi-walled carbon nanotubes (MWCNTs) coated with platinum nanoparticles (Pt-NPs) was prepared as a novel composite nanomaterial by using waste synthetic oil and green chemistry. MWCNT and Pt-NPs were characterised through TEM, FE-SEM, AFM and FT-IR techniques. The diameters of the synthesised MWCNTs and Pt-NPs were 26.80–44.66 and 56.49–89.38 nm, respectively. The formation of MWCNT-COOPt and MWCNT-Pt was confirmed using Raman and EDX techniques. The effect of MWCNT-COO, MWCNT-COOPt and MWCNT-Pt on prostate cancer cell line PC3 was studied by MTT assay at various concentrations following near-infrared (NIR) irradiation (λ=1064 nm, P = 15.3 W) at different time intervals (30, 60, 90 and 120 s). The composite of Pt-NPs upon the MWCNT surface enhanced its ability to absorb NIR radiation, leading to an increase in the temperature of cancer cells due to plasmon phenomenon. The composites were utilised in a novel treatment against human PC3 cell line. The maximum temperatures for MWCNT-COO, MWCNT-COOPt and MWCNT-Pt recorded with 25 μg/mL were 43.4 °C, 45.8 °C and 46.2 °C, respectively, and irradiation time was recorded at 120 s. These compounds exhibited high cytotoxicity towards human PC3 cells (58.6%, 71.6% and 79.6%), respectively. The combination of MWCNTs and Pt-NPs in photothermal therapy has potential to be used in local therapy for prostate cancer in a time- and concentration-dependent manner.

1. Introduction

The National Cancer Institute (NCI) defines cancer as an abnormal growth of cells that tend to proliferate in an uncontrolled manner and can metastasise and invade other tissues. Cancer can arise from different organ structures and develops as a result of abnormal genetic and/or epigenetic events. Prostate cancer is the most common type of cancer in men especially in western countries. It starts with the growth of abnormal cells in the prostate, a male-specific sex organ [1,2].

Cancerous tumours can be treated using a variety of methods, including surgery, radiation, chemotherapy, cryotherapy and high-intensity ultrasound [3,4]. However, the majority of these techniques are only moderately effective and can be return and intrusive. Successful therapeutic approaches, such as supplementary treatments and/or thermal therapy, must be considered to reduce adverse side effects on healthy, non-target tissues and increase the treatment efficacy [5]. Photothermal therapy (PTT) is an effective approach. When photo-absorbers are subjected to near-infrared (NIR) laser, PTT causes tumor death by converting light to heat. PTT can be used as a local therapy for cancer cells in primary tumours or as a treatment for local metastasis [6]. Multifunctional, tuneable nano-based photo absorbers have been investigated in recent decades to increase PTT selectivity, efficiency and heat generation for site-specific cell death. Noble metals, transition metals, sulfide/oxide NPs (semi-conductor, rare-earth ion-doped nanocrystals), carbonaceous NPs and other NIR organic-polymeric nanoagents are among the many forms of photo-absorbing NPs [7,8]. The unique attributes of NPs, including high surface to volume ratios, broad optical properties, simple functionalisation and simple surface chemistry and manufacturing make them an appropriate clinical candidate cancer therapy [9,10]. Furthermore, they can efficiently convert light or radiofrequency into heat, allowing for thermal ablation of targeted tumor cells [11].

PTT has received considerable attention because it is minimally invasive and very successful [12–14]. Carbon materials are theranostic reagents that can be combined with PTT for multimodal imaging. It has high photothermal conversion efficiency and can deliver energy accurately and precisely to target tissues [15]. Organic dyes [16], Noble metal NPs [17], and inorganic nanoparticles

* Corresponding author.
E-mail address: sc.dr.ahmedm.mohammed@uoanbar.edu.iq (A.M. Mohammed).

https://doi.org/10.1016/j.jorganchem.2022.122422
0022-328X/

(NPs) [18] are commonly used. In comparison with noble metals and organic dyes, multi-walled carbon nanotubes (MWCNTs) offer the advantages of great chemical and thermal stability [19], low cost, ease of synthesis and lack of damage to surrounding healthy cells. These materials can also successfully convert near-infrared reflection (NIR) to heat, making them suitable photothermal conversion agents for PTT [20]. PTT involves delivering plasmonic nanoparticles to the tumor and exposing these particles to laser light. It causes the conduction band electrons to oscillate, resulting in the absorption or dispersion of light radiation. The absorbed light is converted to heat, which has an irreversible effect on the surrounding tissues [21]. PTT involves delivering plasmonic NPs to the tumor and exposing these particles to laser light. It causes the conduction band electrons to oscillate, resulting in the absorption or dispersion of light radiation. The absorbed light is converted into heat, which has an irreversible effect on surrounding tissues [22–25].

MWCNTs have been increasingly used because of their unique physical and chemical properties, such as a large surface area, high physical and thermal stability and superior conductivity [5]. MWCNTs are biocompatible and capable of converting NIR photons into heat. MWCNTs can minimize undesirable side effects on healthy tissues, thereby improving anticancer benefits [26]. Si-Pt-NCs displayed significant absorption in the 1000–1200 nm spectral range, confirming their excellent absorbance in the NIR-II window. Individual irradiated Pt NPs with diameter of 50–70 nm may readily achieve surface temperatures of 900 K, as reported by Akbar Samadi, who quantified the exceptional thermoplast capabilities of Pt NPs and evaluated their efficacy in PTT for cancer [27]. Si-Pt-NCs were exposed to 1064 nm laser irradiation and demonstrated a significant concentration-dependent heating impact. The temperature of Si-Pt NCs (0.05 mg mL^{-1}) increased to 54.2 °C from a maximum of 23.5 °C [28]. MWCNTs and Pt-NPs can undergo plasmon resonance under the effect of 1064 nm NIR laser. In the present research, plasmon resonance will be enhanced by Pt-NPs on the MWCNT surface. The composites MWCNT-Pt and MWCNT-COOPt will be used as a new treatment against prostate cancer cell line (PC3) by using PTT and compared with MWCNT-COO under the same conditions.

2. Material and methods

2.1. Materials

Chemicals such as sulphuric acid, nitric acid and chloroplatinic acid hexahydrate [H_2PtCl_6. 6(H_2O)] were purchased from Sigma-Aldrich. Waste synthetic oil was collected from an Iraqi oil refinery. Trypsin/EDTA, RPMI 1640 and foetal bovine serum were obtained from Capricorn (Germany). DMSO was supplied by Santacruz Biotechnology (USA). MTT (3-(4, 5-dimethyl-2-thiazolyl)−2, 5-diphenyl-2H-tetrazolium bromide) was acquired from Bio-World (USA).

2.2. Methods

2.2.1. Preparation of carbon from waste oil

A new system was designed based on the incomplete combustion of oil Fig. 1 for the preparation of carbon from waste synthetic oil. After combustion, carbon was collected from the interior walls of the combustion tank in a fine powder form. The powder was washed and dried for the preparation of MWCNTs.

2.2.2. Preparation of MWCNTs

MWCNTs were manufactured by sonication in a probe working at a frequency of 22 kHz, amplitude of 100 m and power of 100 W. In brief, 1 g of carbon powder was placed in a 250 mL vessel with 100 mL of deionised water. The probe is 6.4 mm in diameter and moved vertically expanding and contracting with the liquid sample. Sonication was performed in cycles of 10 min followed by 1 min rest to allow the sample to cool between the sonication steps. The solution was then centrifuged for 15 min at 6000 rpm before drying for 24 h at 110 °C-120 °C [29,30].

2.2.3. Oxidation of MWCNTs

The aggregation of MWCNT particles in distilled water is a significant constraint in their application. Several approaches have been proposed to address this limitation. An example is connecting the carboxyl group (-COOH) to CNTs. The dispersion of CNTs in water increases as a result of this connection [5]. MWCNT was carboxylated by adding concentrated HNO_3 and H_2SO_4 in a 1:1 ratio. The reaction mixture was sonicated for 1 hour. The 1:1 reaction mixture was refluxed for 3 h at 120 °C, diluted with distilled water and allowed to sediment [31]. The acid treatment not only increased the functionalisation but also shortened the MWCNTs, resulting in less entanglement and improved solubility [32]. A new automated washing system was designed for continuous washing of MWCNT-COO to remove acid wastes Fig. 2. The system was programmed to turn off if the pH of the filtrate water recorded by the pH sensor becomes 7. The pH sensor was programmed to measure pH every 500 ms otherwise the washing process was operated continuously.

2.2.4. Preparation of platinum nanoparticles Pt-NPs using green chemistry

A new automated system was developed for the preparation of Pt-NPs Fig. 3. Eucalyptus leaves were washed with deionised water and dried at 50 °C. The dried leaves were ground to fine powder. About 1 g of the powder was placed in beaker 1 of the system. The beaker was then added with 100 mL of deionised water. When the system was operated, the heater (1) was turned on. When the temperature reached 90 °C, the heater was turned off after 30 min and vacuum filtration started automatically. About 10 mL of the filtrated extract from flask 1 was withdrawn and poured in beaker 2 that was fixed on heater 2. A total of 50 mL of 0.01 M [H_2PtCl_6.6(H_2O)] was also withdrawn from flask 2 and poured in beaker 2. In the third step, heater 2 with magnetic stirrer was turned on. When the temperature reached 90 °C, the heater was turned off after 20 min. Finally, Pt-NPs were obtained using the new system based on green chemistry.

2.2.5. Preparation of MWCNT-Pt-NPs composite

In brief, 250 mg of chitosan powder was dissolved in 50 mL of 4% acetic acid. The mixture was agitated for 30 min by magnetic stirrer and sonicated for 2 h with 100 mg of MWCNT-COO powder. The suspension was then centrifuged at 5000 r/min, and the supernatant was collected. Finally, 1 mL of the Pt-NP elution was combined with 5 mL of the CNT dispersion and sonicated for 30 min to prepare MWCNT-COO-Pt composite Fig. 4A [33].

For the preparation of MWCNT-Pt, 100 mg of MWCNTs were distributed in 40 mL of deionised and ultra-sonicated for 30 min. The suspension was added drop wise with 40 mL of 0.1 M [H_2PtCl_6.6 (H_2O)] aqueous solution. The mixture was then added with 40 mL of eucalyptus extract and ultra-sonicated again for 1 h. Finally, CNT-Pt-NPs were separated from the solution by centrifugation and washed for five times using deionised water Fig. 4B [10].

2.2.6. Characterization of nanoparticles

NPs were characterised by the following techniques. The morphological characterization of NPs at the nanometer and nanoscale levels was carried out using a transmission electron microscope

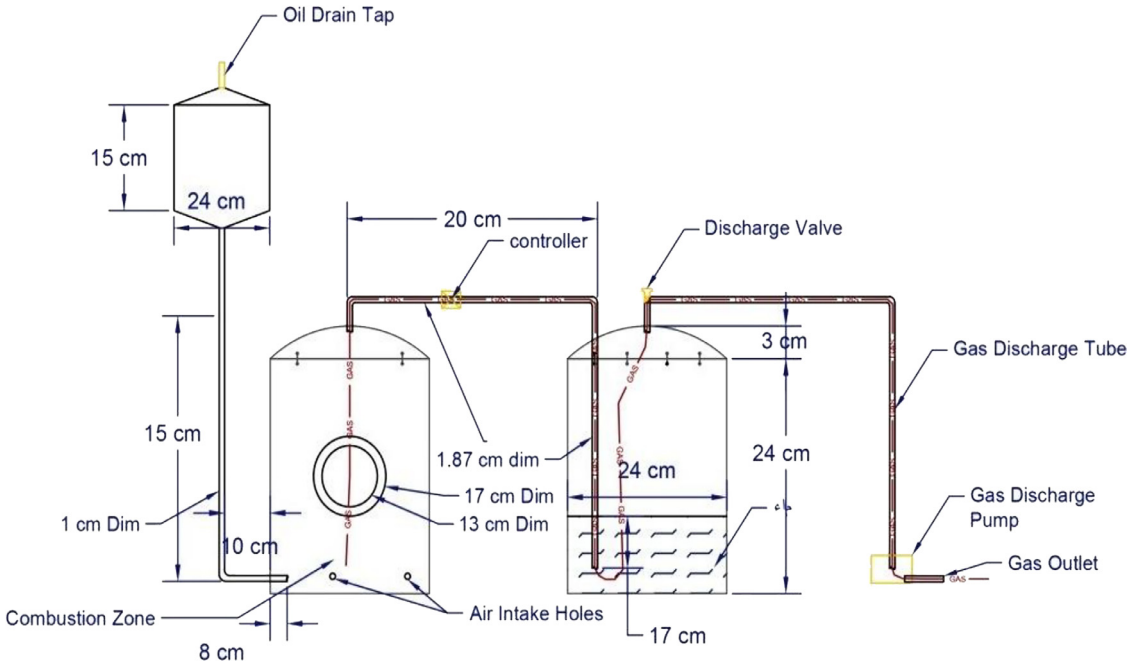

Fig. 1. Schematic diagram of the combustion system.

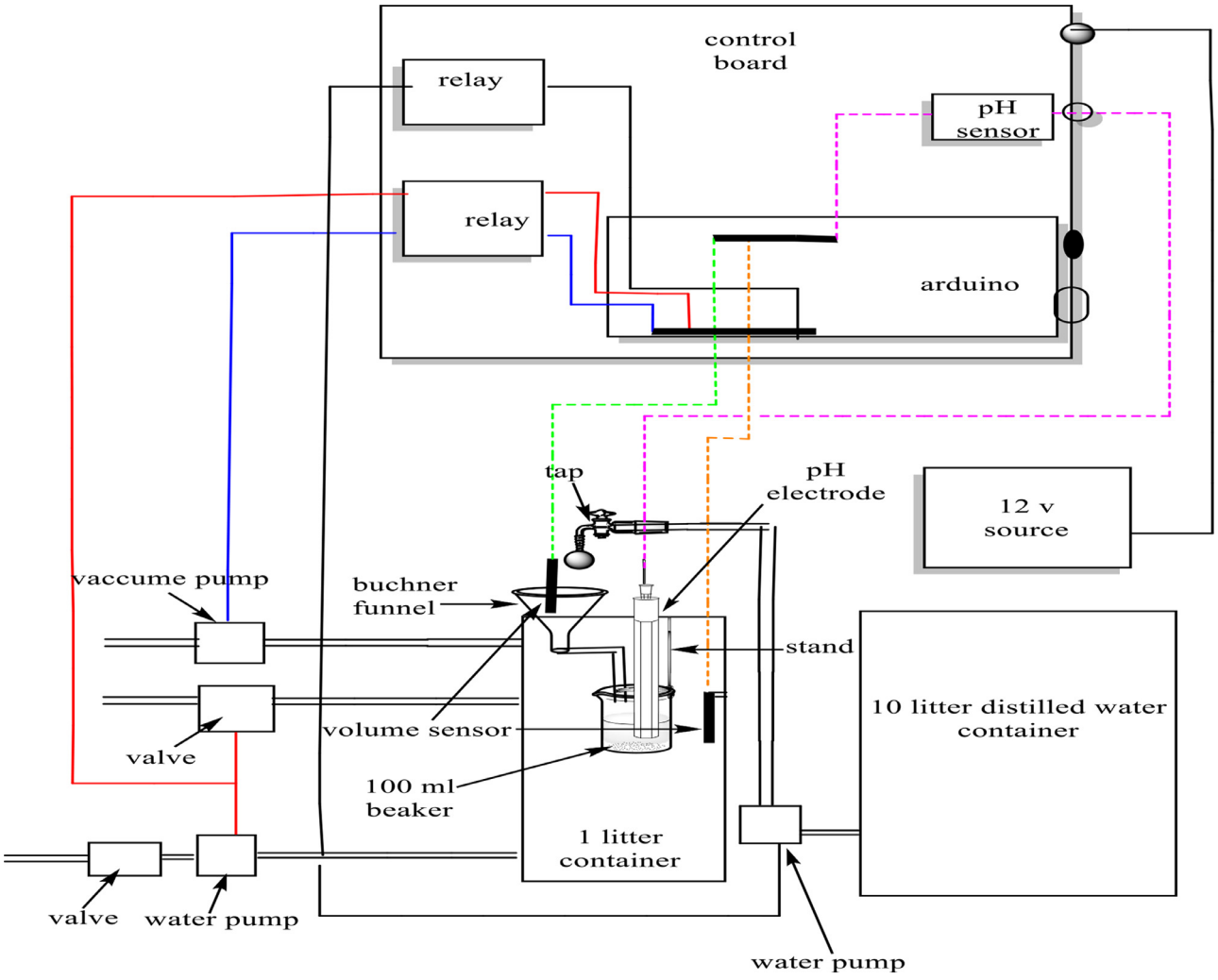

Fig. 2. Schematic diagram of the automatic washing system.

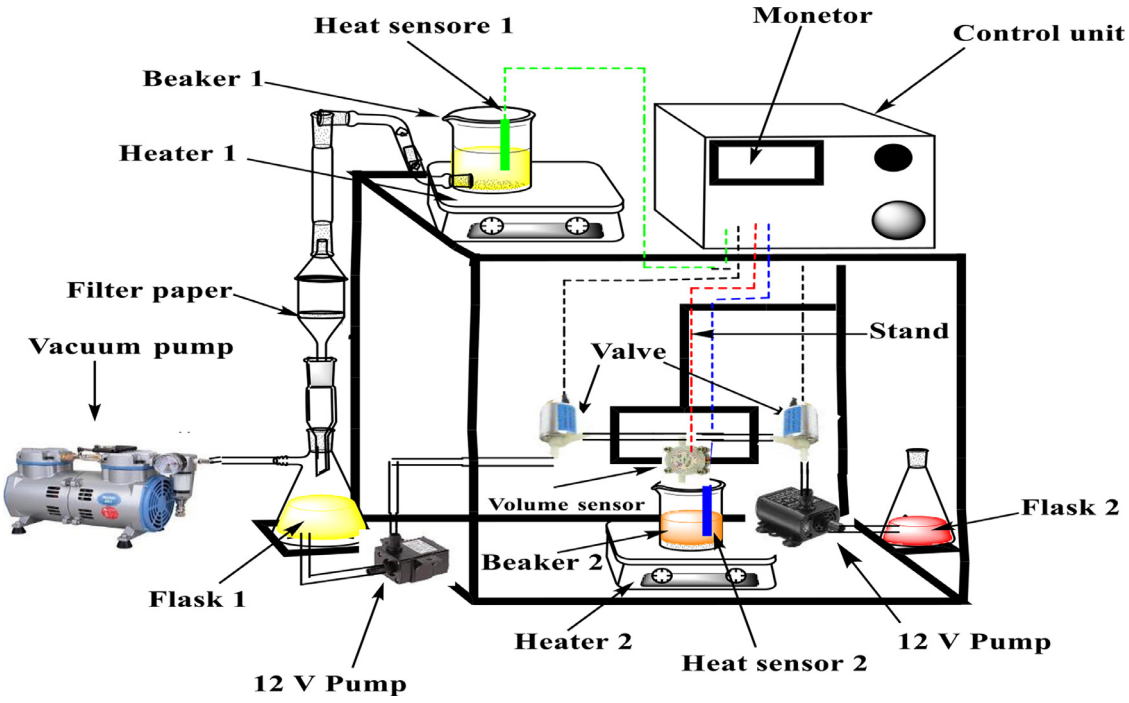

Fig. 3. Schematic diagram of Pt-NPs preparation.

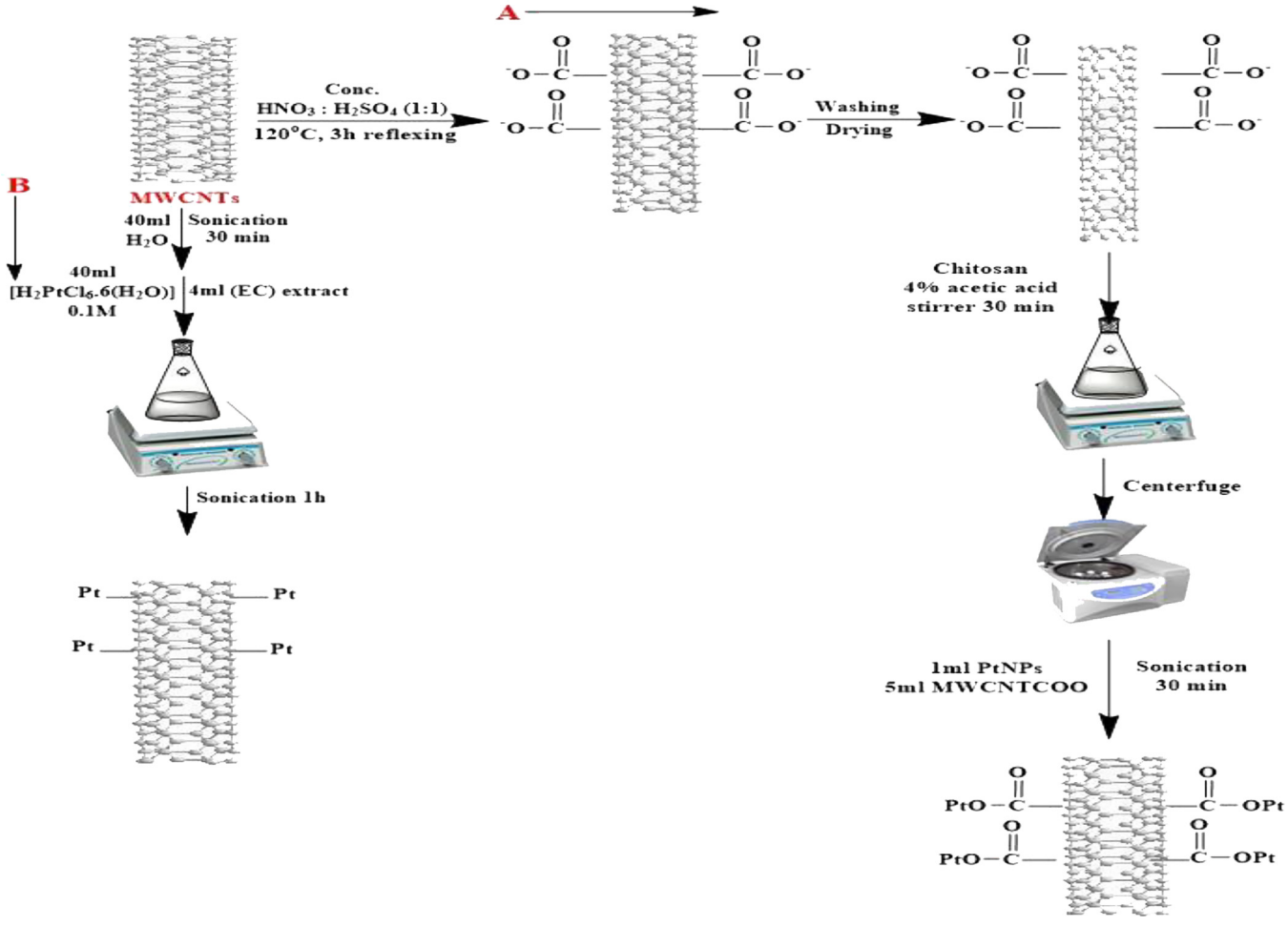

Fig. 4. Mechanism of formation MWCNT-COOPt **(A)** and MWCNT-Pt **(B)**.

(TEM) (Carl Zeiss, Germany) and a field emission scanning electron microscope (FE-SEM). The dimensions of NPs were measured using an atomic force microscope (AFM) (ZEISS Integrated). FT-IR spectroscopy (IRAffinity-1-Shmadzo) was used to analyze the functional groups of NPs. Raman spectra were used to compare nanocomposite encasement works that changed the modes of MWCNT vibration.

2.3. Biological activity of prepared nanomaterials

2.3.1. Anti-cancer activity

2.3.1.1. Maintenance of cell cultures. PC-3 cells were cultured in RPMI-1640 medium supplemented with 10% foetal bovine serum, 100 U/mL penicillin and 100 g/mL streptomycin. The medium was changed twice per week. Cells were passaged with Trypsin-EDTA upon reaching approximately 80% confluence and reseeded into sterile 96-plates for experiment. The cells were then incubated in 5% CO_2 and 95% air at 37 °C [34,35].

2.3.1.2. Cytotoxicity assays. MTT test was used to investigate the cytotoxic effect of NPs on PC3 cell line [35–40]. The cells were cultured using a 96-well microplate at a density of 1×10^4 cells per well. After 24 h or when a confluent monolayer was achieved, the cells were treated with serial concentrations of the prepared composites (3.12, 6.25, 12.5 and 25 µg/mL) for 48 h. The cells with and without NPs were laser irradiated with continuous wave for various periods (30, 60, 90 and 120 s) by using a YLD5–1064-LP (IPG Photonics) ytterbium fiber laser with an intensity of 15.3 W/cm^2 [41]. The medium was discarded from the plate after the exposure time was completed and washed with PBS. About 0.1 mL of MTT working solution dye was added to each well and then incubated for 2.5 h at 37 °C. At the end of the incubation period, the dye was removed from the plate and the wells were washed twice with PBS. Each well was added with 50 µL of DMSO for 15 min at 37 °C to resolve the MIT–formazan crystals [42]. Absorbance was recorded at 492 nm by using a micro-plate reader. The test was performed in triplicate. The following equation was used to compute the percentage of inhibition [43,44].

$$\textbf{Inhibitionrate} = \textbf{A} - \textbf{B}/\textbf{A} * \textbf{100} \quad (1)$$

where A is the mean optical density of the control wells, and B is the mean optical density of the treated wells [45]. The cells were viewed on inverted microscope under 100x magnification, and photographs recorded were recorded using a digital camera mounted to the microscope [46–48].

3. Results and discussion

3.1. Optical and structural characterization

3.1.1. TEM microscopy

Transmission electron microscope was used to examine the morphology of various MWCNTs. The samples were placed in ethyl alcohol and ultrasonically dispersed for 30 min. The sample solution was then placed on a copper grid and allowed to dry before being tested. TEM microscopy was utilised to identify the formation and shape of MWCNTs and Pt-NPs Figs. 5 and 6.

3.1.2. FE-SEM microscopy

The morphology of the nanomaterials was examined using an FSEM device. After brief immersion in liquid nitrogen, all nanomaterials were freeze-fractured and sputter-coated with an Au layer. The FE-SEM spectra shows the formation and surface morphology of MWCNTs and Pt-NPs with diameters of 26.80–44.66 and 56.49–89.38 nm, respectively Figs. 7 and 8.

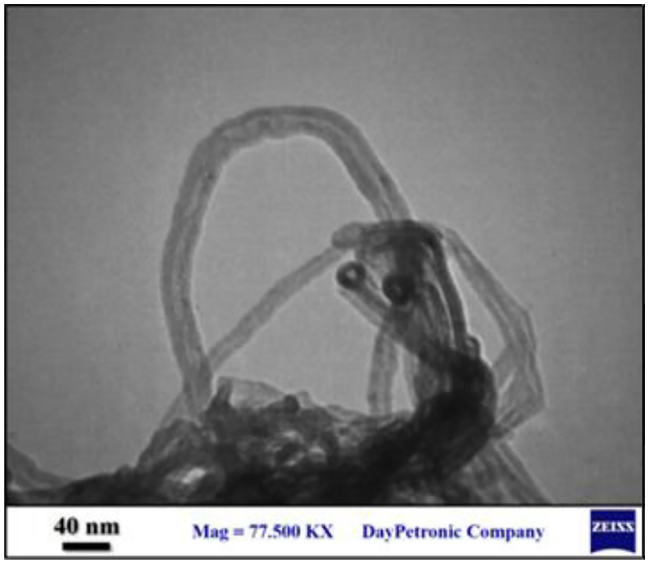

Fig. 5. Shape of MWCNTs using TEM microscopy.

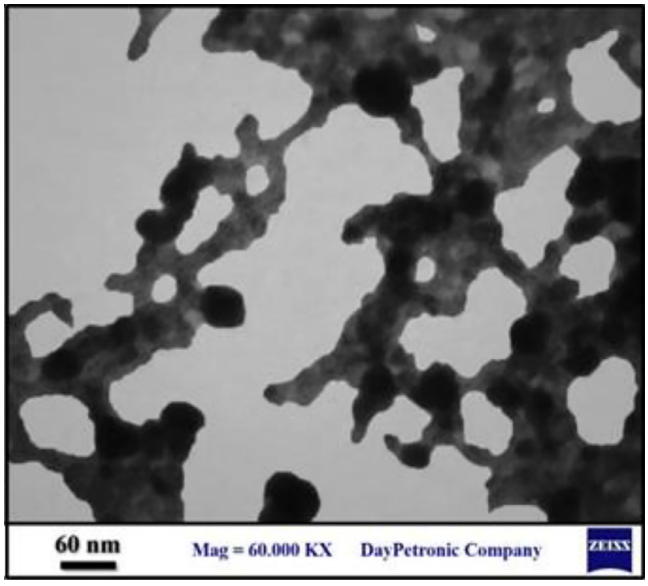

Fig. 6. Shape of Pt-NPs using TEM microscopy.

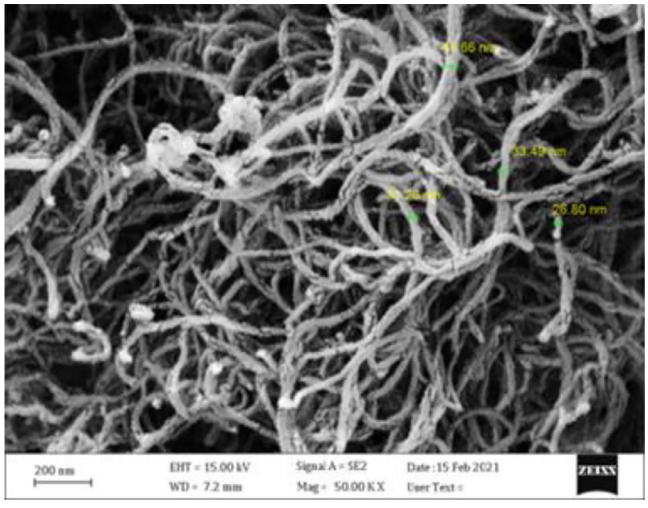

Fig. 7. Surface morphology of MWCNTs using FE-SEM microscopy.

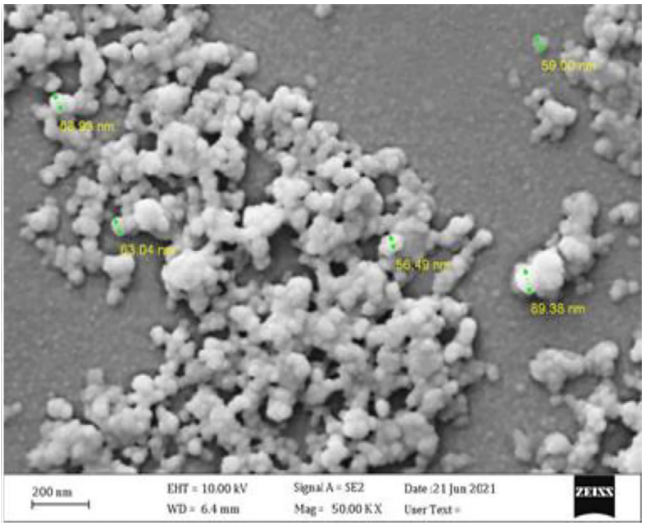

Fig. 8. Surface morphology of Pt-NPs using FE-SEM microscopy.

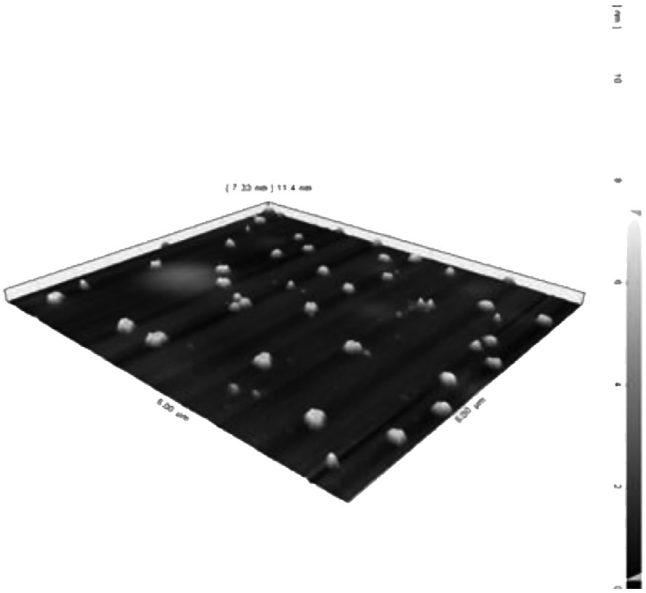

Fig. 9. AFM for MWCNTs.

3.1.3. AFM microscopy

AFM equipment in tapping mode was used to characterize the surface morphology and phase diagram of the nanomaterials. All samples of nanomaterials were chopped into flat pieces to adhere to the sample stage. The flat pieces were then cleaned with ethyl alcohol, dried at 60 °C for 24 h and stored for testing. The three-dimensional surface morphology of MWCNTs and Pt-NPs was determined by AFM microscopy Figs. 9 and 10, respectively. MWCNTs had diameter between 7.33–11.4 nm, and Pt-NPs showed limited distribution with diameter of 30–45 nm.

3.1.4. FT-IR spectrum

The FT-IR spectrum for the prepared MWCNTs showed that the vibration of the carbon skeleton of CNTs is connected with a strong band at 1636 cm^{-1}. The two bands at roughly 2376 cm^{-1} correspond to the stretching vibration of C=C double bonds, which arose from the surface of the tubes Fig. 11. This result is consistent with those obtained by Cunha et al. and Eman et al. [49,50].

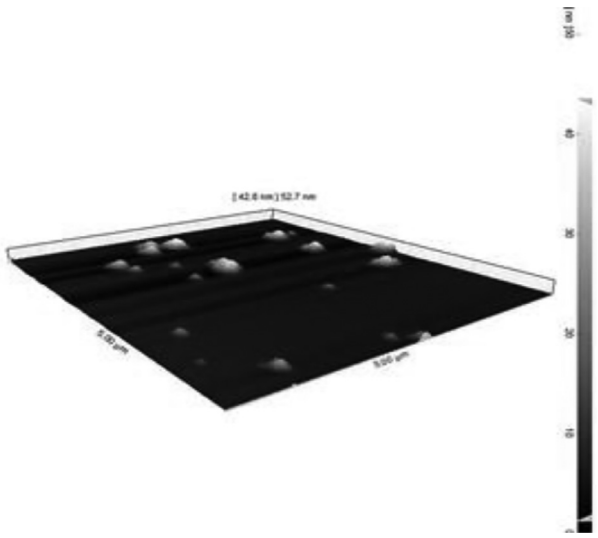

Fig. 10. AFM for Pt-NPs.

3.1.5. Raman spectra

The Raman spectra of MWCNT-Pt, MWCNTCOOPT, MWCNTCOO and MWCNTs were compared to identify how nanocomposite encasement changed the vibration modes of MWCNTs [51]. Fig. 12 shows the Raman spectra of NTs with Pt NPs and unaltered MWCNTs. The Raman spectra for the unmodified MWCNTs revealed the following bands: 1329.32 cm^{-1} band D, 1561.46 cm^{-1} band G and 2661.43 cm^{-1} band H (band 2D). The functional MWCNTs have the following bands: 1335.98, 1335.98 and 1329.32 cm^{-1} for the band D of MWCNTCOO; 1573.65, 1568.28 and 1564.15 cm^{-1} for the band G of MWCNTCOOPT; and 2671.81, 2671.81 and 2663.72 cm^{-1} for the band H (band 2D) of MWCNT-Pt. The intensity of band D in comparison with the normalised band G is the main difference between the two spectra. A spectrum corresponding to MWCNTCOO, MWCNTCOOPT and MWCNT-Pt has the most intense band D. This band is associated with a higher number of defects in the graphite structure of MWCNTs, which are created as a result of the functionalisation the surface of Pt NPs with a mixture of acids. The band G, which corresponds to unaltered MWCNTs, is near 1561.46 cm^{-1}; after functionalisation, it shifts by roughly 12.19, 6.82, 2.69 and 564.15 cm^{-1}. Both spectra show no radial breathing mode (RBM) bands, which are characteristic of single-walled NTs. This finding confirms the presence of MWCNTs and is consistent with the study of Anna D. *et al.* that reported shift by about 7 cm^{-1}[52]. The matching IG/ID ratio was calculated and was found to be 1.04, 1.05, 1.02 and 1.27 for MWCNT, MWCNTCOO, MWCNTCOOPT and MWCNT-Pt, respectively. Thus, using Pt-NPs can significantly reduce graphitic NPs, similar to the study of V. Datsyuka et al. [53].

3.1.6. EDX

The quantity of Pt in each component was revealed by the EDX spectrum of CNT/Pt nanocomposites. MWCNT-COOPt has a lower number of Pt particles adhering to its surface than MWCNT-Pt (Figs. 13 and 14).

3.2. Statistical analysis

All data are expressed using means and standard errors. SPSS program with ANOVA and two-way ANOVA was used for analysis. Statistical significance was determined with a value of <0.05.

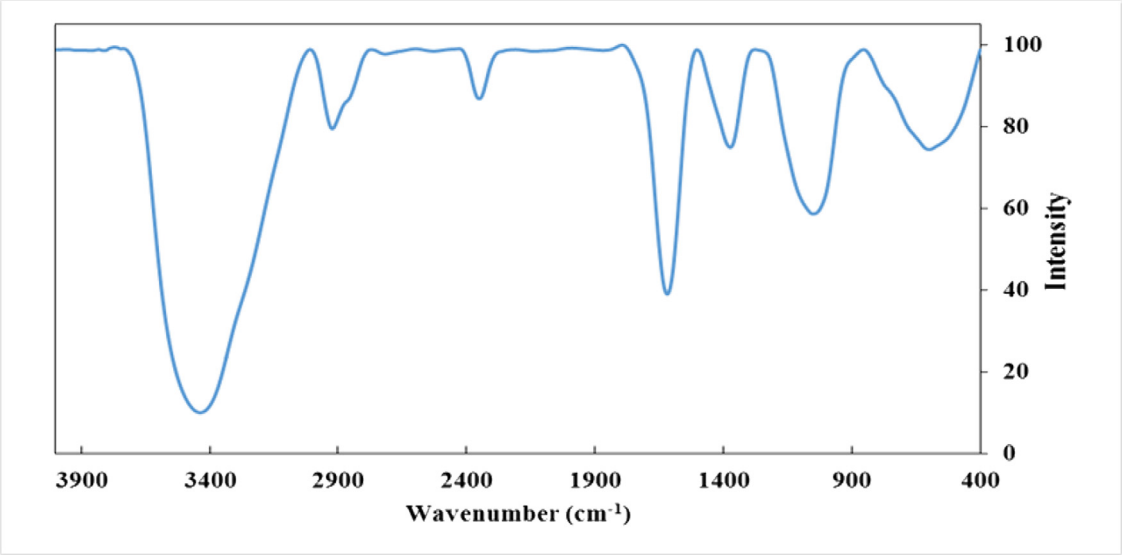

Fig. 11. FT-IR for MWCNTs.

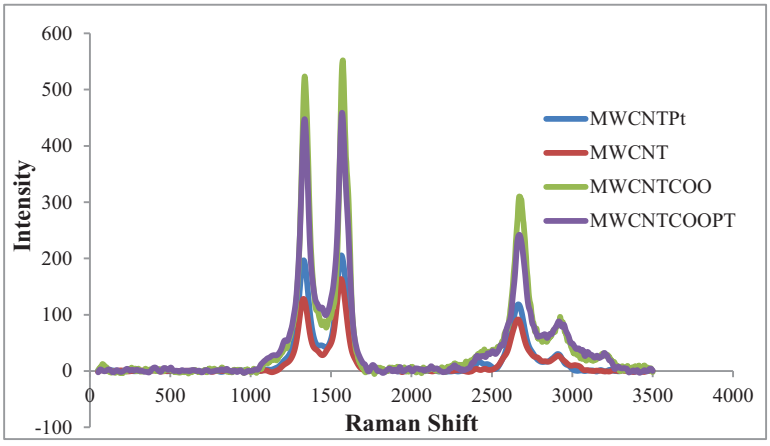

Fig. 12. Raman spectra for composite.

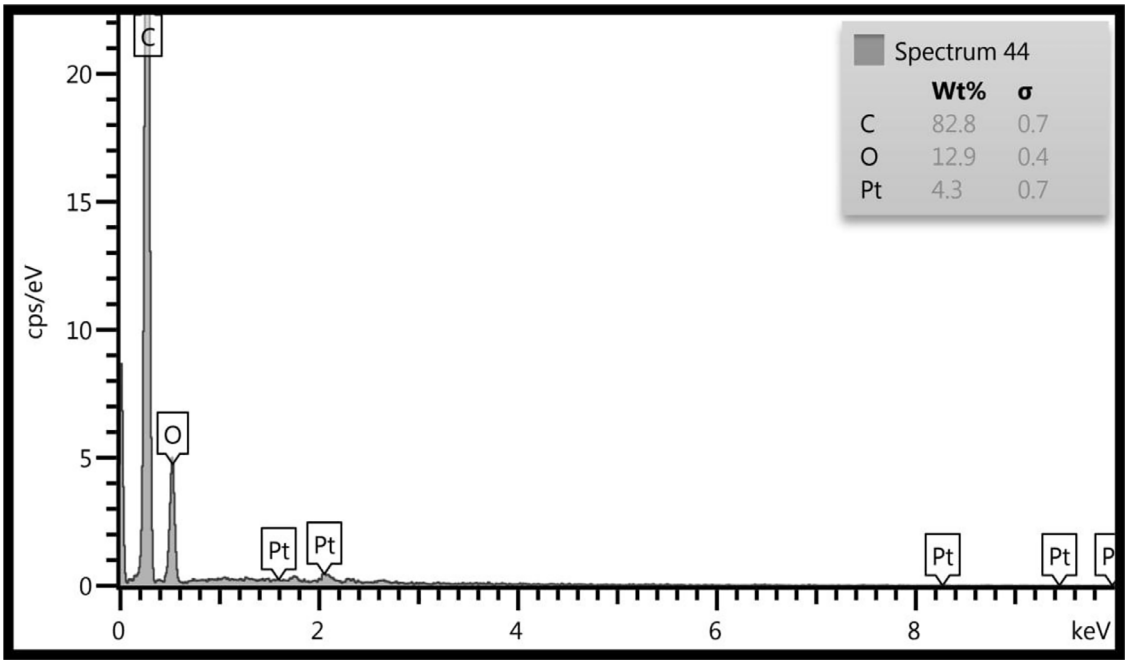

Fig. 13. EDX for MWCNTCOO-Pt.

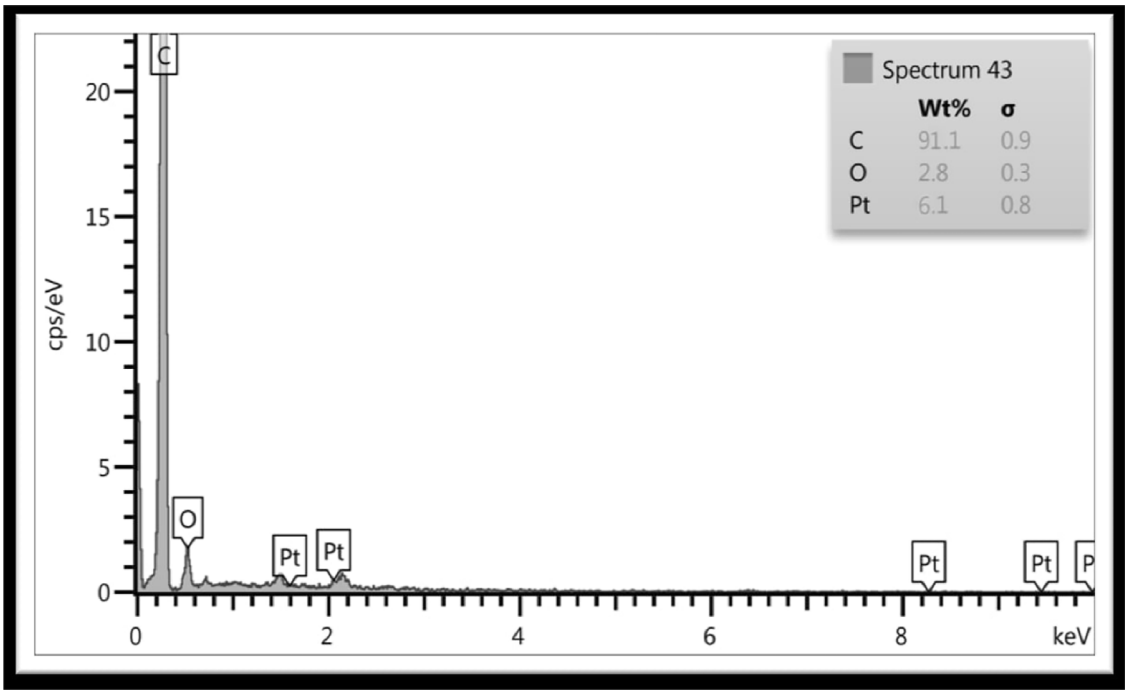

Fig. 14. EDX for MWCNT-Pt.

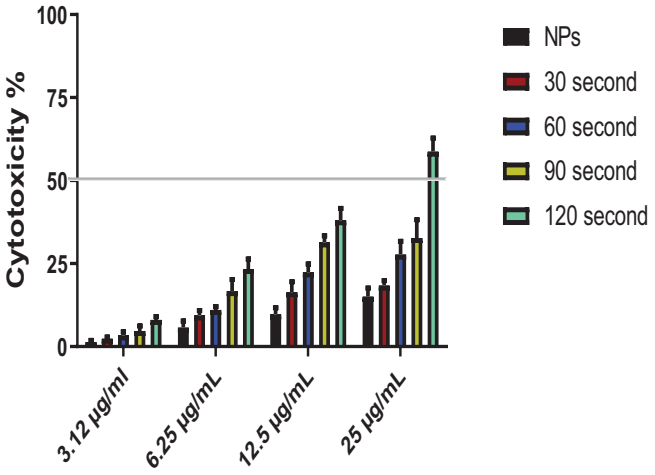

Fig. 15. Cytotoxicity of MWCNT-COO in PC3 cells.

3.3. Cytotoxicity of prepared nanomaterials

3.3.1. Cytotoxicity of MWCNTS-COOH

The concentration and time point for assessing cell cytotoxicity are crucial. Fig. 15 demonstrates the effect of MWCNT-COO on PC-3 cells. MWCNT-COO caused no visible harm to PC3 cells. The cytotoxicity of the combination of MWCNT-COOH and irradiation was then examined. The combination gradually and significantly induced cytotoxicity in PC3 cells in a time and dose-dependent manner. These findings indicate that MWCNT-COOH combined with laser therapy can increase tumor cell death because MWCNTs can successfully absorb NIR light and convert it into heat [54]. Internalised NPs could be triggered at tumor sites by laser irradiation to produce localised heat within 40 °C-45 °C to kill cancer cells [55–57]. NIR radiation is converted into vibrational energy using MWCNTs [58]. As a result, heat created based on laser irritation could increase the temperature of malignant tissues and eliminate tumours [59]. The cells were pretreated with various concentrations of MWCNT-COOH (3.12–25 µg/mL) for 48 h and then exposed to NIR (λ=1064 nm, P = 15.3 W) for various durations (30, 60, 90 and 120 s). Cytotoxicity was assessed by MTT assay. The treatment with the highest dose of MWCNT-COOH (25 µg/mL), resulted in a significant increase in temperature by 6.7 °C after 120 s of irradiation. As a result, the cytotoxicity showed a statistically significant increase of 58.6% in PC3 cells. This temperature elevation is due to heat generated through the excitation of optical transition followed by relaxation in MWCNTs, resulting in increased vibrational frequency modes in the carbon lattice and heating up of the solution. Therefore, MWCNTs can increase the temperature after exposure to 1064 nm [51]. Morphological changes in untreated and treated cells in response to laser heating (NIR) with and without MWCNT-COO are shown in Figs. 18 and 19a and b, respectively. These findings indicate that MWCNT-COOH (3.12–25 µg/mL) in combination with laser therapy can significantly increase the tumor cell death of PC3, suggesting a synergistic effect compared with using each agent alone.

3.3.2. Cytotoxicity of MWCNT-COOPt and MWCNT-Pt

Similar to MWCNT-COO, the cytotoxicity of MWCNT-COOPt or MWCNT-Pt combined with laser irradiation was investigated Figs. 16 and 17. Cells were exposed to 3.12–25 µg/mL MWCNT-COOPt or MWCNT-Pt followed by laser irradiation (λ=1064 nm, P = 15.3 W). A highly synergistic combination effect was found with increasing concentrations of MWCNT-COOPt or MWCNT-Pt at each period. In the absence of NIR, MWCNT-COOPt and MWCNT-Pt had no cytotoxic effect on PC3 cells. By contrast, the cytotoxicity significantly increased in PC3 cells incubated with increasing concentrations of the composites followed by increasing irradiation time. The treatment of cells with 25 µg/mL MWCNT-COOPt increased the temperature by 8.8 °C, thereby significantly increasing the cytotoxicity by 71.66% upon 120 s of laser irradiation. The mean cell cytotoxicity for the MWCNT-Pt was 79.66% at the same concentration and irradiation time due to the increase in temperature by 9.2 °C. The morphological changes in the untreated and treated cells in response to laser heating (NIR) with and without MWCNT-COOPt

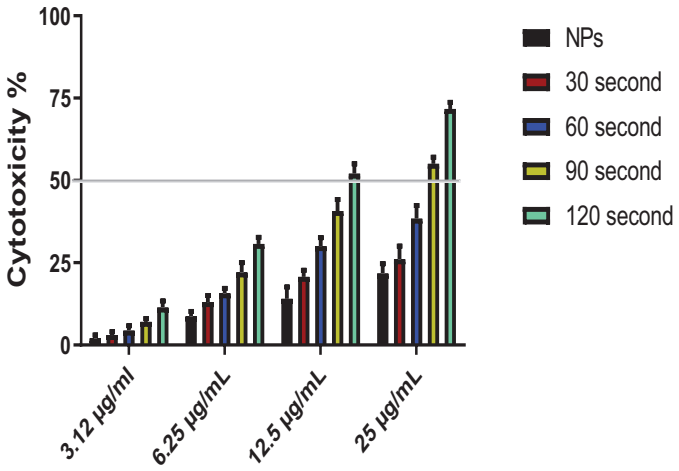

Fig. 16. Cytotoxicity of MWCNT-COO-Pt in PC3 cells.

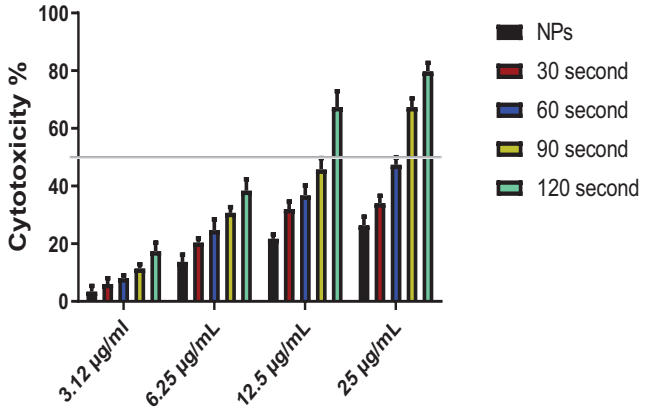

Fig. 17. Cytotoxicity of MWCNT-Pt in PC3 cells.

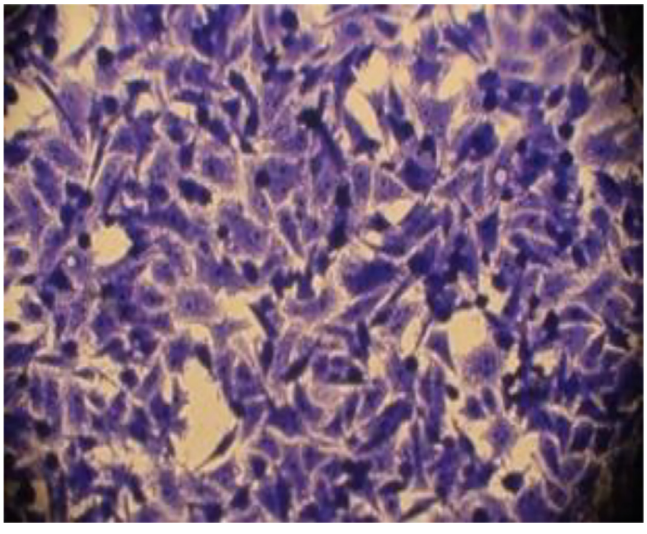

Fig. 18. Control untreated PC3 cells.

and MWCNT-Pt are shown in Figs. 18, 20a and b and 21a and b, respectively. The combined treatment of NIR with MWCNT-COOPt and MWCNT-Pt (3.12–25 µg/mL) significantly induced cytotoxicity in PC3 cells through apoptosis mechanism [60,61], in a dose and time-dependent manner compared with that in non-irradiated control cells.

3.4. Comparison between cytotoxicity of MWCNT-Pt-NPs composites and MWCNT-COOH

Obvious increments in cytotoxicity were found for MWCNT- Pt-NPs and MWCNT-COOPt composites compared with MWCNT-COOH at the same concentration and laser time exposure. This increment may be due to several factors.

Firstly, Pt-NPs contain very strong surface plasmon resonance upon irradiation with off-resonance wavelength especially at 1064 nm. Akbar Samadi et al. reported that irradiation under 1064 nm in the near-infrared (NIR) range led to the maximum temperature higher than those in the other wavelengths. The absorption cross-sections of the 70 and 50 nm wavelengths are the same. Pt-NPs have a peak diameter of 300–400 nm, and the particles are small. Off-resonance has led to irradiation at a wavelength of 1064 nm, resulting in increased surface temperature of Pt-NPs to 720 °C. PT NPs also exhibit exceptional thermo-plasmonic characteristics and efficacy in PTT of cancer [60]. The plasmon PTT rationale of this phenomenon is that plasmonic NPs have useful non-radiative photo-thermal properties. A series of photo-physical reactions can convert the absorbed light into heat [61]. First, the absorbed light is quickly transformed into heat, forming a hot metallic lattice by two processes, namely, electron–electron relaxation and electron–phonon relaxation, which occur in femtoseconds. Even with laser excitation levels as low as 100 nJ, the hot electron temperatures of several thousand degrees Kelvin can be attained in NPs, and lattice temperatures of few tens of degrees can be produced. The lattice cools down as a result of phonon–phonon relaxation. Hence, heat from the particles is dissipated into the surrounding environment, thereby heating the species surrounding the NPs. When NPs are connected to cancer cells, the heat generated by the hot NPs might alter the function of the cells or possibly kill them, depending on the quantity of heat generated [62].

Secondly, the presence of Pt-NPs in compounds results in enhanced absorption of these compounds in the NIR region. The UV–visible absorption of nanocomposites shows that the absorption coefficient increases steadily with increasing amount of Pt-MWCNTs in the composite [63]. The absorption of MWCNTs can be enhanced considerably by increasing the ratio of Pt-NPs in MWCNTs [64]. CNT/Ag NPs absorb light in the 400–1100 nm better than MWCNTs. Mohammad *et al.* demonstrated the unique effects of noble metals on improving the optical absorption of MWCNTs [10]. Therefore, increasing the absorption of NIR can lead to higher production of heat and killing more cancer cells.

Thirdly, the 'nano-attenna' effect may be used to further tune the photophysical properties of MWCNTs by customizing the wall number, diameter and length of the NTs [55]. According to Torte, S. V et al., acidic treatment not only increased the functionalisation but also shortened the MWCNTs [32]. In classical antenna theory, optical coupling of light to NTs is the most efficient for nanotube lengths that are at least half the wavelength of the incident light. Suzy V Torti *et al.* reported that the wavelength of light utilised to activate NTs is less than half the wavelength of CNx-MWNTs at 300 nm (1064 nm) [32]. When the half wavelength of the incident wave equals the length of the slot antenna, the transmittance resonance is expected to occur [65]. The length of MWCNT-COOH may be become less than the half wavelength of the incident wave (1064 nm) due to oxidation; therefore, the amount of heat produce will decrease.

3.5. Comparison between cytotoxicity of MWCNT-COOPt and MWCNT-Pt

The amount of heat produced and the cytotoxicity of MWCNT-Pt are greater than those of MWCNT-COOPt. This finding can be

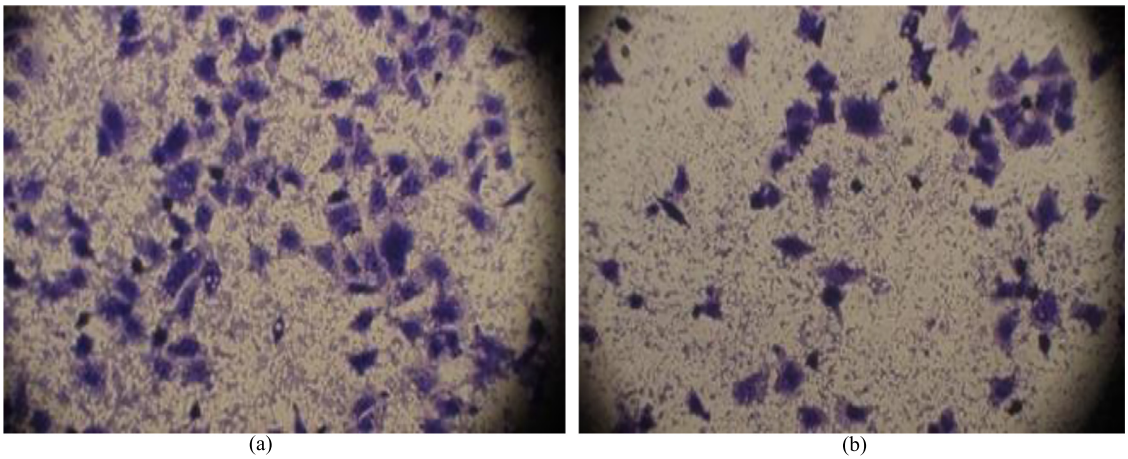

Fig. 19. Morphological changes in PC3 cells **a-** After treatment with MWCNT-COO **b-** After treated with MWCNT-COO and laser.

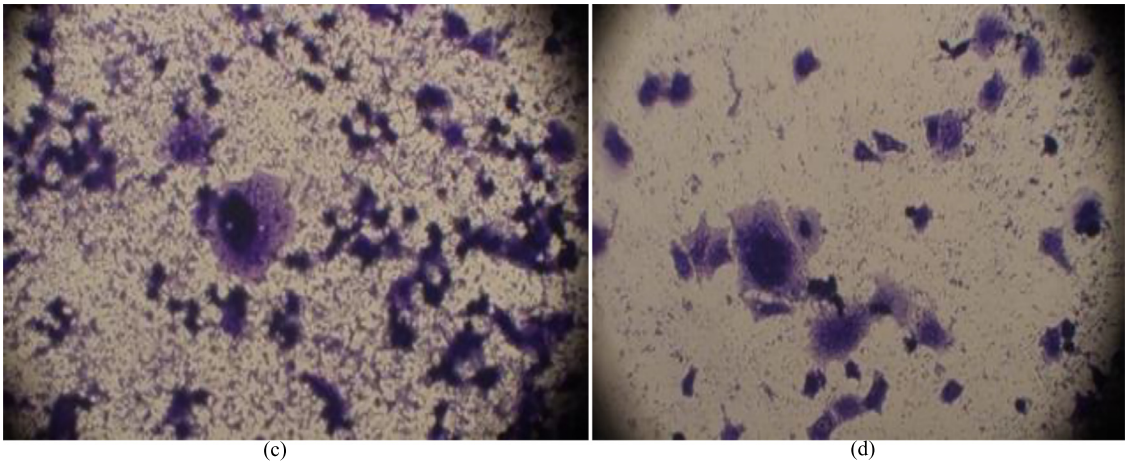

Fig. 20. Morphological changes in PC3 cells **C-** After treated with MWCNT-COOPt
D- After treated with MWCNT-COOPt and laser.

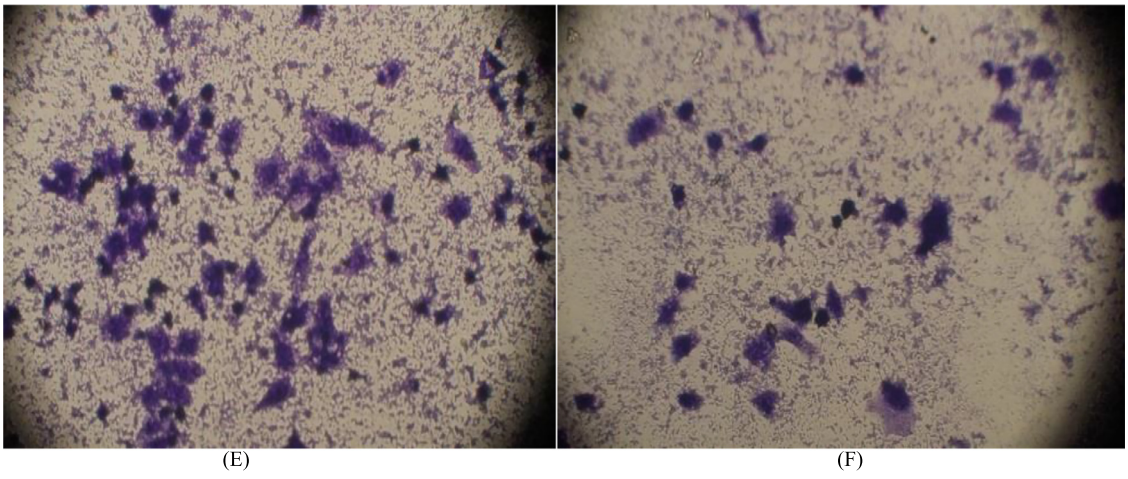

Fig. 21. Morphological changes in PC3 cells **E-**After treated with MWCNT-Pt
F- after treated with MWCNT-Pt and laser.

explained as follows. Firstly, according to Siriviriyanun, the absorption of MWCNTs can be greatly improved by increasing the proportion of Pt-NPs in MWCNTs [64]. The number of Pt-NPs attached to MWCNTs is greater than that attached to MWCNT-COOH. As long as MWCNTs are not treated with acid, they are longer and have more walls; as such, Pt-NP molecules can stick anywhere on the surface of the tubes, leading to higher ratio Fig. 14. As such, MWCNT-Pt have higher ability to absorb radiation and convert it into heat.

Secondly, MWCNTs are functionalised and shortened as a result of the acidic treatment [32]; in this case, Pt-NPs will attach to the COO groups only and will be located on the outermost

Table 1
The values of IC50 for the Nanomaterials at with and without irradiation.

Time of irradiation	IC_{50} forMWCNT-Pt (μM)	IC_{50} forMWCNT-COOPt (μM)	IC_{50} forMWCNT-COO (μM)
0 s.	84.95	99.75	179.1
30 s.	50.47	84.62	170.9
60 s.	25.55	37.02	68.07
90 s.	13.82	19.44	50.84
120 s.	8.494	12.06	18.53

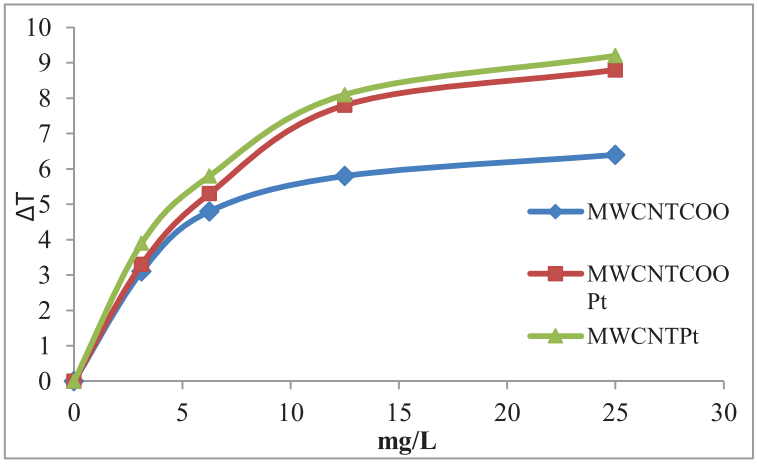

Fig. 22. Effect of concentration of NPs on the elevation of temperature in PC3 cell line at 120 second NIR laser irradiation time.

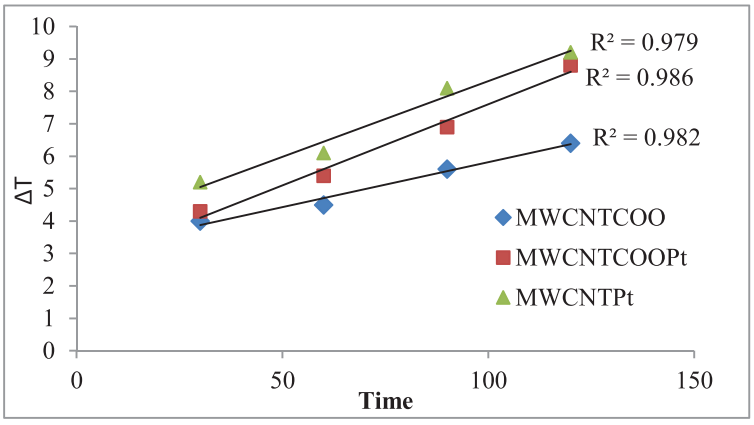

Fig. 23. Effect of NIR laser irradiation time on the elevation of temperature in PC3 cell line at maximum concentrations (25 mg/L).

layer of the MWCNTs. Oxidation leads to the conversion of only a small portion of the carbon atoms in the outer layer of MWCNTs to carboxylic groups. The shorter length of MWCNTs indicates a smaller number of walls and Pt-NPs attached to MWCNTs Fig. 13. Hence, MWCNT-COOPt can absorb less radiation than MWCNT-Pt and also generates low amount of heat. The values of IC50 for the nanomaterials with or without irradiation are recorded in Table 1.

3.6. Effect of concentration on heat elevation

The extent of heating for MWNTCOO, MWCNT-COOPt and MWCNT-Pt was measured to check if the MWCNT composites change the heating efficiency of MWCNTs. In brief, MWCNT composites were irradiated at 1064 nm. The heat difference after and before 120 s of irradiation was recorded among MWNTCOO, MWCNT-COOPt and MWCNT-Pt (3.12–25 μg/mL). Fig. 22 shows that the maximum temperatures recorded were 6.4 °C, 8.8 °C and 9.2 °C for MWNTCOO, MWCNT-COOPt and MWCNT-Pt, respectively.

3.7. Effect of irradiation time on heat elevation

Treatment with the same concentration of the materials but different irradiation times (30–120 s) was conducted to examine the effect of irradiation time on heat elevation. The time was plotted versus the heat difference Fig. 23. The heat elevation is time dependent for MWNTCOO, MWCNT-COOPt and MWCNT-Pt.

4. Conclusion

MWCNTs were synthesised from waste synthetic oil and combined with Pt-NPs to form MWCNT-COO, MWCNT-COOPt and MWCNT-Pt. In our preclinical investigations, MWCNTs coated by Pt-NPs showed great ability to induce the absorption and cytotoxicity of the MWCNTs in the NIR region. The composites showed significant anti-cancer activity and functioned synergistically with radiation therapy (NIR) against prostate cancer cells. The effect is due to increasing temperature by using PTT in a dose and time-dependent manner. These encouraging results provide a basis for subjecting the develop therapy into clinical trials.

Declaration of Competing Interest

The authors have declared no conflict of interest

Acknowledgment

The authors would like to acknowledge the contribution of the University Of Anbar (www.uoanbar.edu.iq) via their prestigious academic staff in supporting this research with all required technical and academic support.

Reference

[1] R. Siegel, E. Ward, O. Brawley, A. Jemal, "Cancer statistics, 2011: the impact of eliminating socioeconomic and racial disparities on premature cancer deaths, CA. Cancer J. Clin. 61 (4) (2011) 212–236.
[2] K.H. Pang, "Molecular strategies to reduce unnecessary repeat prostate biopsies of men with elevated serum PSA." University of Sheffield, 2018.
[3] M.H. Bahreyni-Toosi, M.H. Zare, A. Ale-Davood, M.T. Shakeri, S. Soudmand, In-vitro study of photothermal anticancer activity of carboxylated multiwalled carbon nanotubes, J. Biomed. Phys. Eng. 7 (4) (2017) 317.
[4] N.A. Goushbolagh, B. Farhood, A. Astani, A. Nikfarjam, M. Kalantari, M.H. Zare, Quantitative cytotoxicity, cellular uptake and radioprotection effect of cerium oxide nanoparticles in MRC-5 normal cells and MCF-7 cancerous cells, Bionanoscience 8 (3) (2018) 769–777.
[5] N. Abdi Goushbolagh, M. Keshavarz, M.H. Zare, M.H. Bahreyni-Toosi, M. Kargar, B. Farhood, Photosensitizer effects of MWCNTs-COOH particles on CT26 fibroblastic cells exposed to laser irradiation, Artif. cells, nanomedicine, Biotechnol 47 (1) (2019) 1326–1334.
[6] L. Zou, et al., Current approaches of photothermal therapy in treating cancer metastasis with nanotherapeutics, Theranostics 6 (6) (2016) 762.
[7] A.M. Pekkanen, M.R. DeWitt, M.N. Rylander, Nanoparticle enhanced optical imaging and phototherapy of cancer, J. Biomed. Nanotechnol. 10 (9) (2014) 1677–1712.
[8] S. Govindaraju, K. Yun, Synthesis of gold nanomaterials and their cancer-related biomedical applications: an update, 3 Biotech 8 (2) (2018) 1–13.
[9] G.S.R. Raju, L. Benton, E. Pavitra, J.S. Yu, Multifunctional nanoparticles: recent progress in cancer therapeutics, Chem. Commun. 51 (68) (2015) 13248–13259.
[10] M.A. Behnam, et al., Novel combination of silver nanoparticles and carbon nanotubes for plasmonic photo thermal therapy in melanoma cancer model, Adv. Pharm. Bull. 8 (1) (2018) 49.
[11] H. Sharma, P.K. Mishra, S. Talegaonkar, B. Vaidya, Metal nanoparticles: a theranostic nanotool against cancer, Drug Discov. Today 20 (9) (2015) 1143–1151.
[12] Y. Fu, et al., Luminescent $CaTiO_3$: yb, Er nanofibers co-conjugated with Rose Bengal and gold nanorods for potential synergistic photodynamic/photothermal therapy, J. Mater. Chem. B 5 (26) (2017) 5128–5136.
[13] W. Li, et al., Mild photothermal therapy/photodynamic therapy/chemotherapy of breast cancer by Lyp-1 modified Docetaxel/IR820 Co-loaded micelles, Biomaterials 106 (2016) 119–133.
[14] S. Xu, et al., 808nm laser induced photothermal effect on Sm^{3+}/Nd^{3+} doped NaY $(WO_4)_2$ microstructures, Sensors Actuators B Chem 240 (2017) 386–391.
[15] H. Zhang, et al., Graphene oxide-$BaGdF_5$ nanocomposites for multi-modal imaging and photothermal therapy, Biomaterials 42 (2015) 66–77.
[16] W. He, L. Cheng, L. Zhang, Z. Liu, Z. Cheng, X. Zhu, A versatile Fe_3O_4 based platform via iron-catalyzed AGET ATRP: towards various multifunctional nanomaterials, Polym. Chem. 5 (2) (2014) 638–645.
[17] X. Li, et al., Formation of gold nanostar-coated hollow mesoporous silica for tumor multimodality imaging and photothermal therapy, ACS Appl. Mater. Interfaces 9 (7) (2017) 5817–5827.
[18] T. Liu, et al., Mn-complex modified $NaDyF_4$: yb@ $NaLuF_4$: Yb, Er@ polydopamine core-shell nanocomposites for multifunctional imaging-guided photothermal therapy, J. Mater. Chem. B 4 (15) (2016) 2697–2705.
[19] J. Balamurugan, R. Thangamuthu, A. Pandurangan, Growth of carbon nanotubes over transition metal loaded on Co-SBA-15 and its application for high performance dye-sensitized solar cells, J. Mater. Chem. A 1 (16) (2013) 5070–5080.
[20] J. Sui, et al., Integrating photoluminescence, magnetism and thermal conversion for potential photothermal therapy and dual-modal bioimaging, J. Colloid Interface Sci. 510 (2018) 292–301.
[21] R.S. Riley, E.S. Day, Gold nanoparticle-mediated photothermal therapy: applications and opportunities for multimodal cancer treatment, Wiley Interdiscip. Rev. Nanomed. Nanobiotechnol. 9 (4) (2017) e1449.
[22] D.K. Roper, W. Ahn, M. Hoepfner, Microscale heat transfer transduced by surface plasmon resonant gold nanoparticles, J. Phys. Chem. C 111 (9) (2007) 3636–3641.
[23] J.R. Cole, N.A. Mirin, M.W. Knight, G.P. Goodrich, N.J. Halas, Photothermal efficiencies of nanoshells and nanorods for clinical therapeutic applications, J. Phys. Chem. C 113 (28) (2009) 12090–12094.
[24] H. Chen, et al., Understanding the photothermal conversion efficiency of gold nanocrystals, Small 6 (20) (2010) 2272–2280.
[25] V.P. Pattani, J.W. Tunnell, Nanoparticle-mediated photothermal therapy: a comparative study of heating for different particle types, Lasers Surg. Med. 44 (8) (2012) 675–684.
[26] Z. Zhang, et al., Electrospun PLA/MWCNTs composite nanofibers for combined chemo-and photothermal therapy, Acta Biomater 26 (2015) 115–123.
[27] A. Samadi, H. Klingberg, L. Jauffred, A. Kjær, P.M. Bendix, L.B. Oddershede, Platinum nanoparticles: a non-toxic, effective and thermally stable alternative plasmonic material for cancer therapy and bioengineering, Nanoscale 10 (19) (2018) 9097–9107.
[28] L. Sun, et al., Silicon nanowires decorated with platinum nanoparticles were applied for photothermal-enhanced sonodynamic therapy, Theranostics 11 (19) (2021) 9234.
[29] A.M. Mohammed, I.K. Al-Khateeb, A.J. Haider, R.A. Rahim, U. Hashim, Preparation of DNA biosensor application from fuel oil waste by functionalization and characterization of MWCNT, Sens. bio-sensing Res. 16 (2017) 1–5.
[30] C.S. Davis, J.W. Woodcock, J.W. Gilman, Preparation of nanoscale multi-walled carbon nanotube dispersions in a polyetheramine epoxy for eco-toxicological assessment, NIST Spec. Publ. 1200 (2015) 9.
[31] L. Ravindran, M.S. Sreekala, S. Anilkumar, S. Thomas, Effect of MWCNT carboxylation on mechanical, thermal and morphological behaviour of phenol formaldehyde nanocomposites, J. Compos. Mater. 55 (9) (2021) 1151–1166.
[32] S.V. Torti, et al., Thermal ablation therapeutics based on CNx multi-walled nanotubes, Int. J. Nanomedicine 2 (4) (2007) 707.
[33] X. Jiang, Q. Wang, Refractive index sensitivity enhancement of optical fiber SPR sensor utilizing layer of MWCNT/PtNPs composite, Opt. Fiber Technol. 51 (2019) 118–124.
[34] A.G. Al-Ziaydi, A.M. Al-Shammari, M.I. Hamzah, M.S. Jabir, Hexokinase inhibition using D-Mannoheptulose enhances oncolytic newcastle disease virus-mediated killing of breast cancer cells, Cancer Cell Int. 20 (1) (2020) 1–10.
[35] A.G. Al-Ziaydi, M.I. Hamzah, A.M. Al-Shammari, H.S. Kadhim, M.S. Jabir, The anti-proliferative activity of D-mannoheptulose against breast cancer cell line through glycolysis inhibition, AIP Conf. Proc. 2307 (1) (2020) 20023.
[36] H.N.K. Al-Salman, E.T. Ali, M. Jabir, G.M. Sulaiman, S.A.S. Al-Jadaan, 2-Benzhydrylsulfinyl-N-hydroxyacetamide-Na extracted from fig as a novel cytotoxic and apoptosis inducer in SKOV-3 and AMJ-13 cell lines via P53 and caspase-8 pathway, Eur. Food Res. Technol. 246 (2020) 1591–1608.
[37] N.H. Ali, A.M. Mohammed, Biosynthesis and characterization of platinum nanoparticles using Iraqi Zahidi dates and evaluation of their biological applications, Biotechnol. Rep. 30 (2021) e00635.
[38] B.Y. Hussein, A.M. Mohammed, Green synthesis of ZnO nanoparticles in grape extract: their application as anti-cancer and anti-bacterial, Mater. Today Proc. (2021).
[39] O.H. Abdullah, A.M. Mohammed, Biosynthesis and characterization of MgO nanowires using Prosopis Farcta and evaluation of their applications, Inorg. Chem. Commun. (2020) 108435.
[40] B.Y. Hussein, A.M. Mohammed, Biosynthesis and characterization of nickel oxide nanoparticles by using aqueous grape extract and evaluation of their biological applications, Results Chem. 3 (2021) 100142.
[41] J.W. Fisher, et al., Photothermal response of human and murine cancer cells to multiwalled carbon nanotubes after laser irradiation, Cancer Res. 70 (23) (2010) 9855–9864.
[42] S.H. Kareem, A.M. Naji, Z.J. Taqi, M.S. Jabir, Polyvinylpyrrolidone loaded-MnZnFe 2 O 4 magnetic nanocomposites induce apoptosis in cancer cells through mitochondrial damage and P 53 pathway, J. Inorg. Organomet. Polym. Mater. 30 (12) (2020) 5009–5023.
[43] M.S. Jabir, et al., Green synthesis of silver nanoparticles from Eriobotrya japonica extract: a promising approach against cancer cells proliferation, inflammation, allergic disorders and phagocytosis induction, Artif. Cells Nanomed. Biotechnol. 49 (1) (2021) 48–60.
[44] A.M. Al-Shammari, H. Al-Saadi, S.M. Al-Shammari, M.S. Jabir, Galangin enhances gold nanoparticles as anti-tumor agents against ovarian cancer cells, AIP Conf Proc 2213 (1) (2020) 20206.
[45] M.S. Jabir, et al., Green synthesis of silver nanoparticles using annona muricata extract as an inducer of apoptosis in cancer cells and inhibitor for $NLRP_3$ inflammasome via enhanced autophagy, Nanomaterials 11 (2) (2021) 384.
[46] K.S. Khashan, F.A. Abdulameer, M.S. Jabir, A.A. Hadi, G.M. Sulaiman, Anticancer activity and toxicity of carbon nanoparticles produced by pulsed laser ablation of graphite in water, Adv. Nat. Sci. Nanosci. Nanotechnol. 11 (3) (2020) 35010.
[47] M. Jabir, et al., Linalool-loaded glutathione-modified gold nanoparticles conjugated with CALNN peptide as apoptosis inducer and NF-κB translocation inhibitor in SKOV-3 cell line, Int. J. Nanomed. 15 (2020) 9025.
[48] A.M. Sameen, M.S. Jabir, M.Q. Al-Ani, Therapeutic combination of gold nanoparticles and LPS as cytotoxic and apoptosis inducer in breast cancer cells, AIP Conf. Proc. 2213 (1) (2020) 20215.
[49] C. Cunha, et al., Hybrid composites made of multiwalled carbon nanotubes functionalized with Fe_3O_4 nanoparticles for tissue engineering applications, Nanotechnology 23 (46) (2012) 465102.
[50] A.M. Eman, M. Dawya, A. Abouelsayedb, I. Elsabbaghc, M. Elfassc, Synthesis and characterization of multi-walled carbon nanotubes decorated ZnO nanocomposite, Egypt. J. Chem 59 (2016) 1061–1068.
[51] S. Ghosh, et al., Increased heating efficiency and selective thermal ablation of malignant tissue with DNA-encased multiwalled carbon nanotubes, ACS Nano 3 (9) (2009) 2667–2673.
[52] A.D. Dobrzańska-Danikiewicz, D. Łukowiec, Synthesis and characterization of Pt/MWCNT s nanocomposites, Phys. Status Solidi 250 (12) (2013) 2569–2574.
[53] V. Datsyuk, et al., Chemical oxidation of multiwalled carbon nanotubes, Carbon N. Y. 46 (6) (2008) 833–840.

[54] Y. Hashida, et al., Photothermal ablation of tumor cells using a single-walled carbon nanotube–peptide composite, J. Control. Rel. 173 (2014) 59–66.
[55] R. Singh, S.V. Torti, Carbon nanotubes in hyperthermia therapy, Adv. Drug Deliv. Rev. 65 (15) (2013) 2045–2060.
[56] H. Banu, et al., Doxorubicin loaded polymeric gold nanoparticles targeted to human folate receptor upon laser photothermal therapy potentiates chemotherapy in breast cancer cell lines, J. Photochem. Photobiol. B Biol. 149 (2015) 116–128.
[57] T. Sadhukha, T.S. Wiedmann, J. Panyam, Inhalable magnetic nanoparticles for targeted hyperthermia in lung cancer therapy, Biomaterials 34 (21) (2013) 5163–5171.
[58] J. Liu, et al., Mesoporous silica coated single-walled carbon nanotubes as a multifunctional light-responsive platform for cancer combination therapy, Adv. Funct. Mater. 25 (3) (2015) 384–392.
[59] J.L. Roti Roti, Cellular responses to hyperthermia (40-46) °C: cell killing and molecular events, Int. J. Hyperth. 24 (1) (2008) 3–15.
[60] A. Burke, et al., Long-term survival following a single treatment of kidney tumors with multiwalled carbon nanotubes and near-infrared radiation, Proc. Natl. Acad. Sci. 106 (31) (2009) 12897–12902.
[61] S. Link, M.A. El-Sayed, Optical properties and ultrafast dynamics of metallic nanocrystals, Annu. Rev. Phys. Chem. 54 (1) (2003) 331–366.
[62] X. Huang, M.A. El-Sayed, Plasmonic photo-thermal therapy (PPTT), Alexandria J. Med. 47 (1) (2011) 1–9.
[63] E.A.M. Farrag, R.A. Abdel-Rahem, S.S. Ibrahim, A.S. Ayesh, Electrical and optical properties of well-dispersed MWCNTs/PVA nanocomposites under different pH conditions, J. Thermoplast. Compos. Mater. 32 (4) (2019) 442–453.
[64] A. Siriviriyanun, T. Imae, Advantages of immobilization of Pt nanoparticles protected by dendrimers on multiwalled carbon nanotubes, Phys. Chem. Chem. Phys. 14 (30) (2012) 10622–10630.
[65] Y.-.M. Bahk, D.J. Park, D.-.S. Kim, Terahertz field confinement and enhancement in various sub-wavelength structures, J. Appl. Phys. 126 (12) (2019) 120901.